

Chapter 10

Light-Emitting Field-Effect Transistors with π -Conjugated Liquid Crystalline Polymer

Hisao Yanagi, Yusuke Ohtsuka, Tatsuya Muneishi, and Atsushi Ishizumi

10.1 Introduction

10.1.1 Organic Light-Emitting Field-Effect Transistor

Along with commercialization of organic light-emitting diodes (OLEDs) (Tang and VanSlyke 1987; Sheats et al. 1996), much attention has now been paid on practical applications of organic optoelectronic devices such as organic field-effect transistors (OFETs) (Kudo et al. 1984) and organic photovoltaic (OPV) cells (Tang 1986). In OLEDs, the active layers are mostly composed of amorphous films of vapor-deposited small molecular species. In order to make more use of organic materials advantages, such as low cost, low temperature processing, and flexibility, further efforts have been made to develop polymeric thin film devices which are accessible by wet and printable processes (Broughes et al. 1990; Tsumura et al. 1986). On the other hand, OFET researches have been extensively performed with polycrystalline films of pentacene molecules (Kelly et al. 2003) and higher carrier mobility performances was reported for single crystals of small molecular materials such as rubrene (Takeya et al. 2007). In recent years, high-mobility OFETs comparable to single-crystal devices have also been reported for solution-processed polymeric films one after another.

In conjunction with the research progresses of OLEDs and OFETs, novel organic thin film devices, organic light-emitting field-effect transistors (OLEFETs), have been developed. This device combines charge carrier transport and light-emitting functions in a single device by using fluorescent molecular films as the active layer of OFET. The first successful OLEFET has been reported for vacuum-deposited tetracene films (Hepp et al. 2003). Then, polymeric OLEFETs have also

H. Yanagi (✉) • Y. Ohtsuka • T. Muneishi • A. Ishizumi
Graduate School of Materials Science, Nara Institute of Science and Technology, 8916-5
Takayama, Ikoma, Nara 630-0192, Japan
e-mail: yanagi@ms.naist.jp

been achieved by solution-casting methods (Ahles et al. 2004; Sakanoue et al. 2004). Under ambipolar carrier injection regime, a virtual p/n junction is formed in the channel between the source and drain electrodes by applying appropriate gate voltages. Transported electrons and holes from the opposite electrodes are recombined inside the channel and light emission occurs in a narrow line (Swensen et al. 2005; Zaumseil et al. 2006; Yamane et al. 2007). The line-shaped emission zone can be controlled to be apart from the electrodes, therefore, a quenching loss of emitted light at the electrode interface is reduced. Since the ambipolar channel is formed in a few-nm-thick layer of the active layer in contact with the dielectric surface, high density carriers flow within such a thin channel region. Single-crystal tetracene and rubrene OLEFETs demonstrated current density of several kA cm^{-2} by assuming one monolayer of accumulation thickness (Takenobu et al. 2008). Moreover, the maximum current density of 33 kA cm^{-2} was attained for a single-crystal OLEFET of a thiophene/phenylene co-oligomer (TPCO) (Sawabe et al. 2012).

10.1.2 Towards Organic Semiconductor Laser

Such an achievement of high current density in OLEFETs envisages us to realize organic semiconductor lasers (OSLs) by using molecular single crystals. Moreover, lateral propagation and linear confinement of the high-density carriers seem to be favorable to construct OSLs (Baldo et al. 2002). In fact, organic lasing has already been achieved under optical excitation for a number of small-molecular single crystals (Fichou et al. 1997; Horowitz et al. 1998; Ichikawa et al. 2005) as well as polymeric amorphous films (Tessler et al. 1996; Hide et al. 1996). However, organic lasing under electrical pumping is still challenging and no research has been succeeded yet by using OLEFETs. With an increase of current density beyond $\sim 1 \text{ kA cm}^{-2}$, the luminance of emitted light is rolled off. This is considered to be caused by annihilation processes among singlet, triplet excitons and polarons (Baldo et al. 2002) if high-density excited species are generated in such a low-dimensionally confined region of a few-nm scale. By contrast, the thickness of single-crystal cavity composed of those small molecules is typically a few μm , therefore, a sufficient number of excitons required for optical gain is not generated throughout the whole single-crystal medium under the ambipolar carrier injection regime. Consequently, the principle criteria of lasing with light amplification above a certain threshold of current density has not yet been observed.

In order to overcome such insufficient exciton accumulation within the active layer for OSL, alternate current (AC) gate operation of OLEFETs has been proposed (Yamao et al. 2008). Under the usual DC-gate operation, the ambipolar carrier injection occurs in a specific range of gate biases near the threshold voltages where the source-drain current by simultaneously injected electrons and holes is decreased as compared to that in unipolar transport regime. In the AC-gate operation, on the other hand, electrons and holes are alternately injected from oppositely

biased source and drain electrodes, respectively, and are diffused in the channel of crystal cavity. Electrons (holes) recombine with holes (electrons) which are accumulated in the previous half cycle of the AC gate voltage. The first AC-gate operation proposed by Yamao et al. (2008) was performed for a single-crystal OLEFET with TPCO. Under sinusoidal wave gate bias, the device exhibited an evolution of electroluminescence (EL) when the gate amplitude and frequency were increased. After this first demonstration of AC-gate operation, light-emitting performance has been improved by applying square-wave gate voltages to the single-crystal TPCO device (Yamao et al. 2010). The quick switch of the gate polarity in the square wave enabled efficient carrier recombination so that intense electroluminescence peaks were observed at each instance when the gate polarity changed. This light-emitting recombination under the AC-gate operation which may occur in thicker region of the single-crystal channel is favorable for efficient light emission towards OSL. Actually, Yamao et al. (2010) observed a narrowed emission peak in its electroluminescence spectrum under the square-wave AC-gate operation at 20 kHz. Although it needs to further confirm that this emission is really gain-narrowed with a certain threshold, this result noteworthy envisages us to realize organic lasers by this method.

10.1.3 *Light-Emitting Liquid-Crystalline Polymer*

Those single-crystalline media of small molecules like TPCOs are promising candidates for OSL owing to their high carrier mobility and light confinement structure with an excellent cavity quality. However, those molecular single crystals are very fragile and difficult to be directly grown on the substrate of OLEFET in particular with controlled dimensions for practical device fabrication. Therefore, the AC-gate operation should be also applied to polymeric materials for future flexible light-emitting devices. In view of these research backgrounds, we have started investigating the AC-gate operation of polymeric OLEFETs. Among a variety of light-emitting polymeric semiconductors, we have employed a liquid crystalline co-polymer consisting of π -conjugation with thiophene/fluorene units. Resembling TPCO which is a co-oligomer species of π -conjugating thiophene/phenylene, the thiophene/fluorene co-polymer exhibits ambipolar characteristics (Zheng et al. 2007). In particular, the π -conjugating backbone modified with side alkyl chains crystallize in a nematic phase. This liquid crystallization causes parallel orientation of the thiophene/fluorene planes which promotes carrier transport along the stacking direction of those π -electronic planes. On this basis, ambipolar carrier transports and electroluminescence were demonstrated for those copolymer thin films under conventional DC-operation of OLEFETs (Kajii et al. 2010). According to the reported energy levels of the highest occupied molecular orbital (HOMO) and lowest unoccupied molecular orbital (LUMO) of the thiophene/fluorene copolymer, the energy barrier for electron injection is higher than that for hole injection. Therefore, the light-emitting recombination is typically

obtained in the hole enhancement mode where the accumulated holes recombine with electrons at the drain electrode edges. For further progress of this liquid-crystalline co-polymer OLEFETs, we have investigated ambipolar characteristics and light-emitting behaviors under a variety of conditions of AC-gate operations for spin-coating thin films which are thermally annealed to different crystalline phases (Ohtsuka et al. 2012; Muneishi et al. 2014).

10.2 Preparation and Characterization of Liquid-Crystalline Polymer

10.2.1 Thin Film Preparation

As a liquid-crystalline thiophene/fluorene co-polymer, we chose poly [(9,9-dioctylfluorenyl-2,7-diyl)-co-bithiophene] (F8T2, Fig. 10.1a). A commercially available grade of F8T2 (Aldrich, $M_n > 20,000$) was used without further purification. Prior to thin film preparation, thermal properties of the F8T2 sample was examined by differential scanning calorimetry (DSC). The F8T2 powder exhibited a glass transition at $T_g = 125.5$ °C, and thermotropic transitions to the nematic phase at $T_m = 259.3$ °C and to the isotropic one at $T_i = 311.6$ °C. These phase transitions are almost identical to those reported in the literature (Kinder et al. 2004). For thin film preparation, 5.0 mg of F8T2 powder was dissolved in 1 mL chloroform. The solution was spin-coated on a substrate at 3000 rpm for 60 s. A glass slide ($10 \times 10 \times 1.1$ mm³) coated with indium-tin-oxide (ITO) was used as substrate. The ITO coating was served as a conductive electrode in the following OLEFET fabrication (Fig. 10.1b). According to the DSC result, the F8T2 films was annealed at specific temperatures in a range of 80–350 °C. After keeping for 30 min at the respective temperature, the film was cooled to room temperature at a rate of -60 °C/min in nitrogen.

10.2.2 Optical Characterization

During those thermal annealing processes, we observed morphological changes of the F8T2 films by in situ polarized transmission optical microscopy using an Olympus BX-51 microscope with a heating stage under nitrogen gas flow. The films at 80 and 150 °C showed completely dark images under the cross-Nicole polarization suggesting that those films were amorphous without containing any crystalline domains. When the annealing temperature was increased to 250 °C, ordering of polymer chains started to occur in the film so that the image showed partially transmitted regions. Further increase to 290 °C changed the image exhibiting bright grain structure with the nematic liquid-crystalline phase. With

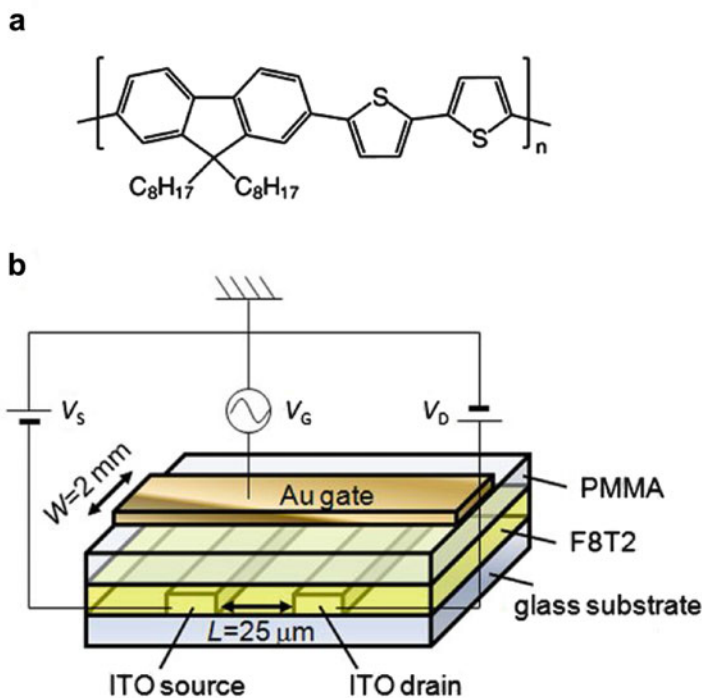


Fig. 10.1 Molecular structure of F8T2 (a) and schematic diagram of bottom-contact/top-gate OLEFET structure (b). Reproduced from Muneishi T, Ishizumi A, Yanagi H (2014) Annealing effect on light-emitting FET characteristics of π -conjugated liquid crystalline polymer. *Jpn. J. Appl. Phys.* 53: 01AB17 with permission from The Japan Society of Applied Physics

elevating annealing temperature up to 350 °C, the image turned dark again indicating that the film melted to an isotropic phase. After cooling to room temperature, the thickness of thus heat-treated F8T2 films was measured to be about 50 nm by a thickness profiler (Tenchor Alpha-Step). Temperature-dependent film structures of those cooled samples were also examined by optical microscopy. Figure 10.2 shows transmission micrographs under the cross-Nicole polarization for the F8T2 films annealed at 250, 290, and 350 °C, and then cooled to room temperature. The dark image in Fig. 10.2a indicates that the film annealed at 250 °C is almost amorphous although some portion of the film was crystallized. By contrast, the films annealed at 290 °C shows bright transmission as shown in Figs. 10.2b. The film consists of microcrystalline grains with a size of $\sim 10 \mu\text{m}$ suggesting that the quenching from this temperature gives rise to formation of the nematic phase. As compared to the dark image under in situ observation during annealing at 350 °C, the film cooled from 350 °C shows homogeneous transmission as shown in Fig. 10.2c. It indicates that the film crystallizes in homogeneous structure with finer grains when the film is quenched from the isotropic phase at 350 °C.

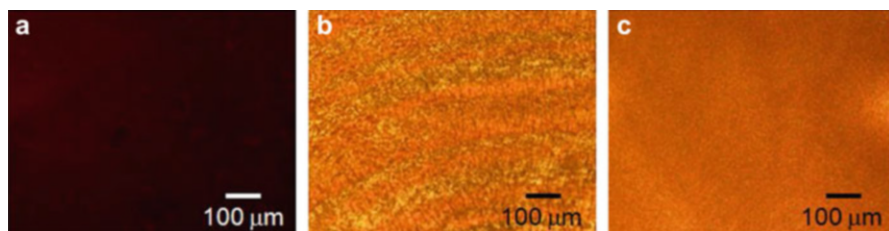


Fig. 10.2 Transmission optical micrographs of the F8T2 films annealed at 250 (a), 290 (b), and 350 °C (c) taken with cross-Nicole polarization. Reproduced from Muneishi T, Ishizumi A, Yanagi H (2014) Annealing effect on light-emitting FET characteristics of π -conjugated liquid crystalline polymer. *Jpn. J. Appl. Phys.* 53: 01AB17 with permission from The Japan Society of Applied Physics

10.2.3 Crystalline Structure

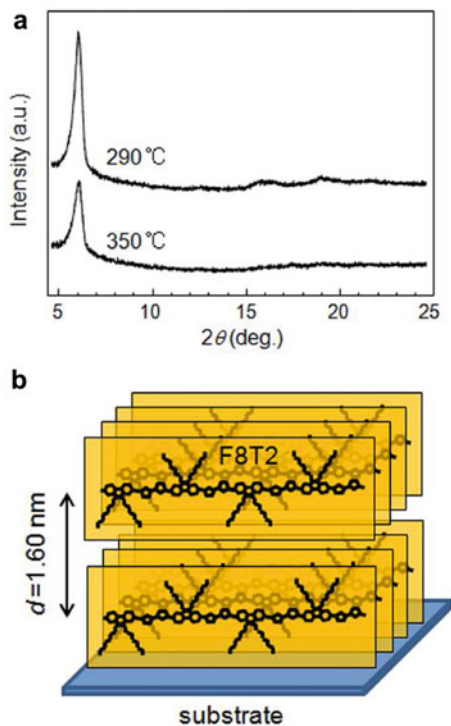
Crystalline structures of those F8T2 films were examined by X-ray diffraction (XRD) using an X-ray diffractometer (Rigaku, RINT-TTRIII/NM). Figure 10.3a shows $2\theta/\theta$ patterns of the films quenched from the annealing temperatures of 290 and 350 °C. Both patterns exhibit a single peak at 5.5° which corresponds to $d = 1.6$ nm. This spacing arises from the interchain distance between the stacked F8T2 lamellae in which the F8T2 chains are lying parallel on the substrate plane. According to these crystallographic observations by polarized optical microscopy and XRD, the film structure is estimated as is schematically shown in Fig. 10.3b. In the film quenched from 290 °C (Fig. 10.2b), the nematic domains are crystallized with this lamellae structure. Due to formation of these microcrystalline grains, this film contains a number of grain boundaries which affect the OLEFET characteristics as mentioned in the following section. On the other hand, there is no remarkable grains in the film annealed at 350 °C (Fig. 10.2c) suggesting that the quenching from the isotropic temperature formed less ordered fine crystallites in homogeneous morphology.

10.3 Light-Emitting Field-Effect Transistor with Liquid-Crystalline Polymer

10.3.1 Device Fabrication and Measurement Methods

Bottom-contact/top-gate OLEFET devices were fabricated as schematically shown in Fig. 10.1b. Onto a glass substrate ($1.0 \times 1.0 \times 1.1$ cm²), ITO coating with a resistivity of 9–15 Ω/sq is patterned in stripes of 200 μm width and 200 nm thickness. The gap between the ITO stripes is 25 μm . A pair of stripe-patterned ITO is served as the source/drain electrodes. After ultrasonic cleaning with

Fig. 10.3 (a) XRD patterns of the F8T2 films annealed at 290 and 350 °C. (b) Schematic diagram of presumed molecular alignment in the F8T2 film. Reproduced from Muneishi T, Ishizumi A, Yanagi H (2014) Annealing effect on light-emitting FET characteristics of π -conjugated liquid crystalline polymer. Jpn. J. Appl. Phys. 53: 01AB17 with permission from The Japan Society of Applied Physics



detergent, deionized water, acetone and ethanol, the ITO/glass surface was treated by UV/ozone exposure. As mentioned in the previous section, the F8T2 solution was spin-coated on the ITO/glass surface at 3000 rpm for 60 s. The casted film was annealed at 80, 150, 250, 290, and 350 °C in nitrogen gas flow for 30 min. After cooling to room temperature, the thickness of the deposited film was measured to be about 50 nm by a thickness profiler (Tenchor Alpha-Step). To construct the top-gate device, the F8T2 film was covered with a dielectric layer of polymethyl methacrylate (PMMA). A 900 mg/10 mL propylene glycol monomethyl ether acetate (PGMEA) solution of PMMA was spin-coated at 3000 rpm for 60 s. After drying at 80 °C for 30 min in nitrogen, the thickness of the PMMA film was 700–850 nm. On top of the PMMA dielectric layer, a gold (Au) film (2 mm wide and ~30 nm thick) was vacuum-deposited as a gate electrode. Consequently, the fabricated OLEFET has bottom-contact ITO source/drain electrodes with channel length $L = 25 \mu\text{m}$ and a Au top-gate channel with channel width $W = 2 \text{ mm}$ as schematically shown in Fig. 10.1b.

Field effect transistor and light-emitting characteristics were measured at room temperature in vacuum. The fabricated device was loaded in a chamber equipped with three tungsten needle probes and evacuated in a vacuum of 10^{-5} mbar. DC current–voltage output and transfer characteristics were measured using a semiconductor characterization system (KEITHLEY 4200). For AC-gate operations, a

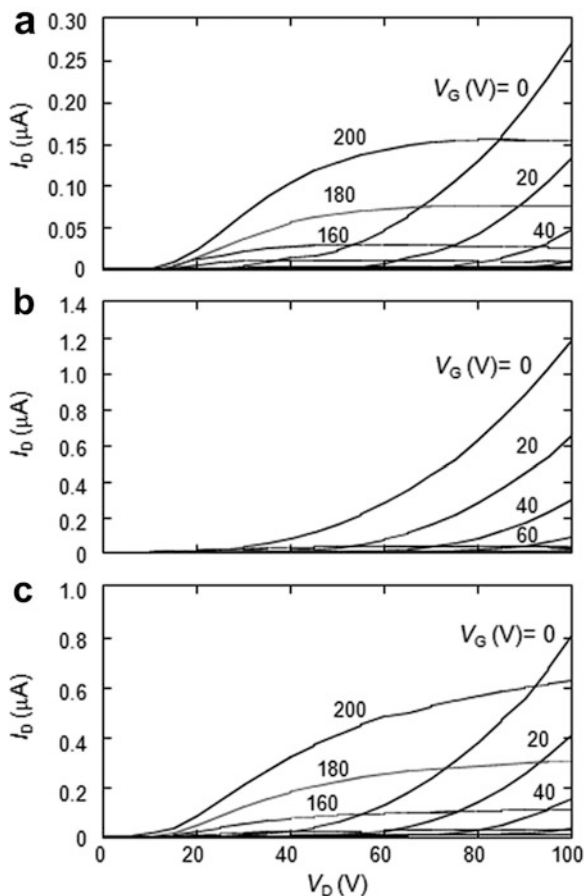
bi-polar power supply (Matsusada POPF120-2.5) and two DC power supplies (Takasago EX-375 L2) were connected as is shown with a circuit diagram in Fig. 10.1b. Electroluminescence (EL) was observed through a top window of the chamber using a stereo microscope (Olympus SZX-12) with a long WD objective lens (Mitsutoyo M Plan Apo 10x). The light intensity was measured with a photomultiplier (Hamamatsu Photonics R1477-561). Time responses of the light intensity was recorded as a function of the AC-gate voltage waves using a digital multimeter (Advantest R6551) and a digital oscilloscope (Tektronics TDS 3052B).

10.3.2 Transistor Characteristics Under DC Operation

The field-effect transistor characteristics of the OLEFET devices fabricated with different F8T2 films were first characterized under DC-gate operations. Figure 10.4 shows output characteristics of the F8T2 films quenched from annealing temperatures of 250, 290 and 350 °C. Drain current (I_D) was plotted as a function of drain voltage (V_D) under positive gate voltage (V_G) varying from 0 to 200 V. When the V_D was positively swept at constant V_G lower than 100 V, the positive I_D increased with an elevation of V_D for all three films. This I_D - V_D behavior is attributed to hole transport from the drain to the source electrode. When V_G is increased beyond 100 V, this hole current is extinct and the I_D - V_D curves change to the saturation regime at higher V_D due to electron injection from the source electrode. With increasing V_D , the drain current is saturated since the electron channel is pinched off when the V_D increases close to V_G . For the films annealed at 250 and 350 °C (Fig. 10.4a, c, respectively), this electron transport is clearly seen with saturated currents which are comparable to the hole currents observed at lower V_G . It demonstrates that these F8T2 films have well-balanced ambipolar characteristics. By contrast, the electron current is very low for the film annealed at 290 °C (Fig. 10.4b) indicating that unipolar hole transport is dominant in this film.

The hole and electron mobility (μ_h and μ_e) are estimated from the saturated regime of I_D for the F8T2 films annealed at different temperatures and summarized in Fig. 10.5a. The hole transport was obtained for all films and μ_h was estimated from the hole saturation regime of $V_D < 0$ and $V_G < 0$: $\mu_h = 2.5 \times 10^{-4}$, 6.4×10^{-5} , 2.5×10^{-4} , 9.7×10^{-4} and 9.8×10^{-4} cm² V⁻¹ s⁻¹ for the films annealed at 80, 150, 250, 290 and 350 °C, respectively. Electron transport was not obtained for the films annealed at 80 and 150 °C probably because their random chain conformation formed by annealing at lower temperature does not enable intermolecular electron hopping. The electron transport was observed when the film is annealed above 250 °C: $\mu_e = 7.8 \times 10^{-5}$, 4.4×10^{-5} and 3.7×10^{-4} cm² V⁻¹ s⁻¹ for the films annealed at 250, 290 and 350 °C, respectively. The μ_h of the film annealed at 350 °C is as same as that at 290 °C while its μ_e remarkably increased as compared to that at 250 °C. The μ_e of the film annealed at 290 °C slightly decreased in comparison with the film annealed at 250 °C while its μ_h increased four times as high as that at 250 °C.

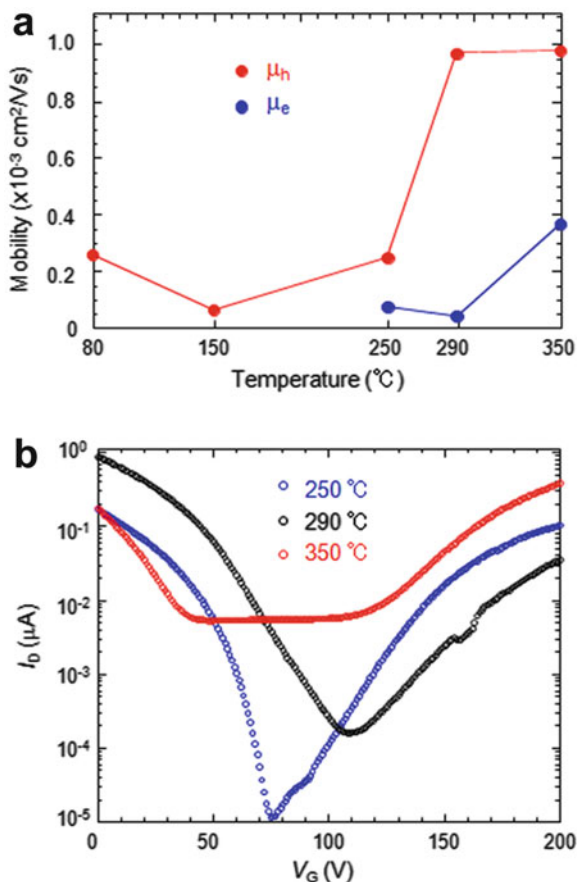
Fig. 10.4 Output characteristics of OLEFETs with the F8T2 films annealed at 250 (a), 290 (b), and 350 °C (c). Reproduced from Muneishi T, Ishizumi A, Yanagi H (2014) Annealing effect on light-emitting FET characteristics of π -conjugated liquid crystalline polymer. Jpn. J. Appl. Phys. 53: 01AB17 with permission from The Japan Society of Applied Physics



The observed ambipolarity for the present bottom-contact/top-gate device is owing to the PMMA dielectric layer which prevents electron trapping. However, it is noted that the threshold voltage for electron injection is considerably higher than that for hole injection estimated in the electron and hole enhancement mode, respectively. This difference is attributed to the HOMO and LUMO energies of F8T2 with respect to the electronic energy of the source/drain ITO electrodes. From the reported values of $E_{\text{HOMO}}/E_{\text{LUMO}} = -5.6/-3.2$ and $E_{\text{ITO}} = -4.8$ eV (Hamasaki et al. 2009), there is a higher injection barrier to electrons than to holes.

In Fig. 10.5b transfer characteristics are compared at $V_D = 100$ V for the F8T2 films annealed at 250, 290 and 350 °C. The I_D of the film annealed at 290 °C is remarkably lower in the electron transport regime at $V_G > 100$ V while the highest hole current is obtained at the low V_G region for this film. It is reported that the electron transport is blocked at grain boundaries (Koiwai et al. 2011). As seen in Fig. 10.2b, the F8T2 film quenched from the nematic phase at 290 °C formed a large number of boundaries among the microcrystalline grains. On the other hand,

Fig. 10.5 (a) Dependence of carrier mobilities in the F8T2 films on annealing temperatures from 80 to 350 °C. (b) Transfer characteristics of OLEFETs with the F8T2 films annealed at 250, 290, and 350 °C. Reproduced from Muneishi T, Ishizumi A, Yanagi H (2014) Annealing effect on light-emitting FET characteristics of π -conjugated liquid crystalline polymer. Jpn. J. Appl. Phys. 53: 01AB17 with permission from The Japan Society of Applied Physics



the hole currents decreased for the film annealed at 250 °C while its electron current increased as compared to that of the film annealed at 290 °C, resulting in a balanced ambipolar transport. This ambipolar behavior is also obtained for the film annealed at 350 °C with further increase of electron currents. It suggests that the entangled polymer chains in the polycrystalline film quenched from the isotropic phase at 350 °C promote in particular electron hopping. The microcrystalline structure in the film annealed at 250 °C has also ambipolar characteristics with well-balanced electron and hole currents when the gate voltages are appropriately applied for each carrier injection. However, its I_D value remarkably falls in the order of 10^{-5} μ A at the voltage where the transfer characteristics change from hole transport regime to electron one. It suggests that the microcrystalline boundaries are also obstacle for carrier transport in particular at insufficient bias voltages.

The dependences of obtained carrier mobilities and transfer characteristics on annealing temperature suggest that the crystalline structure in the annealed films differently affect the transport of holes and electrons. Basically both carrier transports are improved by crystallization within the grains. In particular, the μ_h is

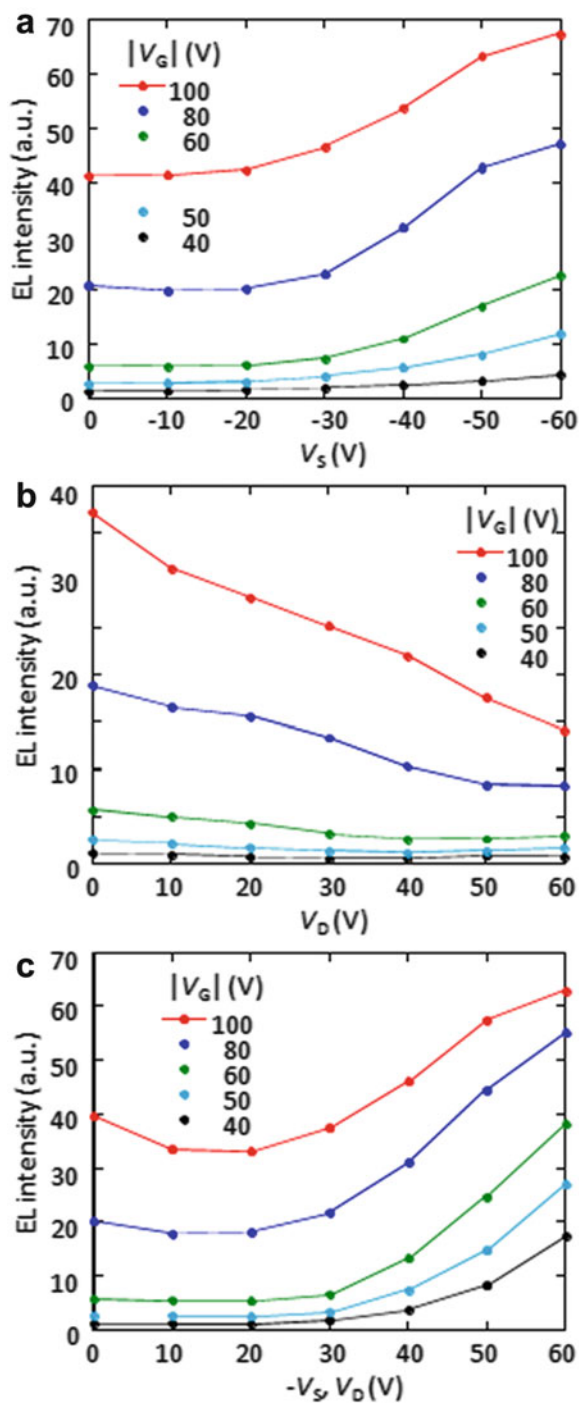
increased by interchain ordering and not sensitive to grain boundaries formed at higher annealing temperature. By contrast, the μ_e is considerably lowered by electron trapping at the grain boundaries in the microcrystalline film quenched from the liquid-crystalline phase annealed at 290 °C. As a consequence, the crystalline film with the nematic structure shows deteriorated ambipolar characteristics as compared to the less crystalline films annealed at 250 and 350 °C.

10.3.3 Light-Emitting Characteristics Under AC-Gate Operation

As mentioned in the previous section, transfer characteristics of the OLEFETs (Fig. 10.5b) indicate that the ampipolar currents when electrons and holes are simultaneously injected are quite low in the wide region of V_G . Therefore, the light intensity was very weak under those conditions of DC-gate operations. Brighter light emission was obtained in the hole enhancement mode where the accumulated holes recombine with electrons injected at the drain electrode edge. On the other hand, under AC-gate operation a large number of holes and electrons can be alternately injected from appropriately biased source and/or drain electrodes resulting in light emission by recombination of accumulated geminate carriers. Hereafter, the fabricated OLEFETs were investigated under AC-gate operations.

Since it is expected that light-emitting performances depend on ambipolar characteristics, the AC-gate operation was carried out under different conditions of source/drain voltages, gate amplitude, gate waveform, and gate frequency using F8T2 films annealed at 350 °C. It is reported that electroluminescence is enhanced when a square wave AC voltage is applied to the gate electrode instead of a sinusoidal wave (Yamao et al. 2008, 2010). In the present study, therefore, light emission properties of the OLEFETs were measured under square-wave gate operations. Figure 10.6 shows dependences of light intensity on V_S and V_D under the square-wave gate frequency at $f=20$ kHz and amplitudes at $|V_G|=40, 50, 60, 80$ and 100 V. As shown in Fig. 10.6a, the V_S is first negatively biased from 0 to -60 V at $V_D=0$ V. Unexpectedly, light emission was obtained when the source and drain electrodes were not biased, i.e. $V_S=V_D=0$ V. The light intensity does not increase with decreasing V_S up to -20 V. Further negative biasing of $V_S < -20$ V increases the light intensity since the electron injection from both edges of the source electrode increases. On the other hand, the light intensity decreases as the V_D is positively biased at $V_S=0$ V in particular at higher $|V_G|$ as shown in Fig. 10.6b. The positive V_D bias remarkably decreases the electron injection from the drain electrode. When the negative V_S and positive V_D are applied with the same amplitude, the light intensity is first kept constant then increases with an elevation of $|V_S|$ and $|V_D|$ at $|V_G|=40, 50$ and 60 V as seen in Fig. 10.6c. When the $|V_G|$ is increased to 80 and 100 V the light intensity first decreases at $|V_S|=|V_D|=0-10$ V, and then increases at $|V_S|=|V_D| > 20$ V. These

Fig. 10.6 Dependences of light intensity on V_S at $V_D=0$ V (a), on V_D at $V_S=0$ V (b) and on $-V_S=V_D$ (c) obtained from OLEFET with F8T2 film annealed at 350 °C at different $|V_G|$. Reproduced from Ohtsuka Y, Ishizumi A, Yanagi H (2012) Light-emitting field-effect transistors with π -conjugated liquid-crystalline polymer driven by AC-gate voltages. *Org. Electron* 13: 1710–1715 with permission from Elsevier B.V.

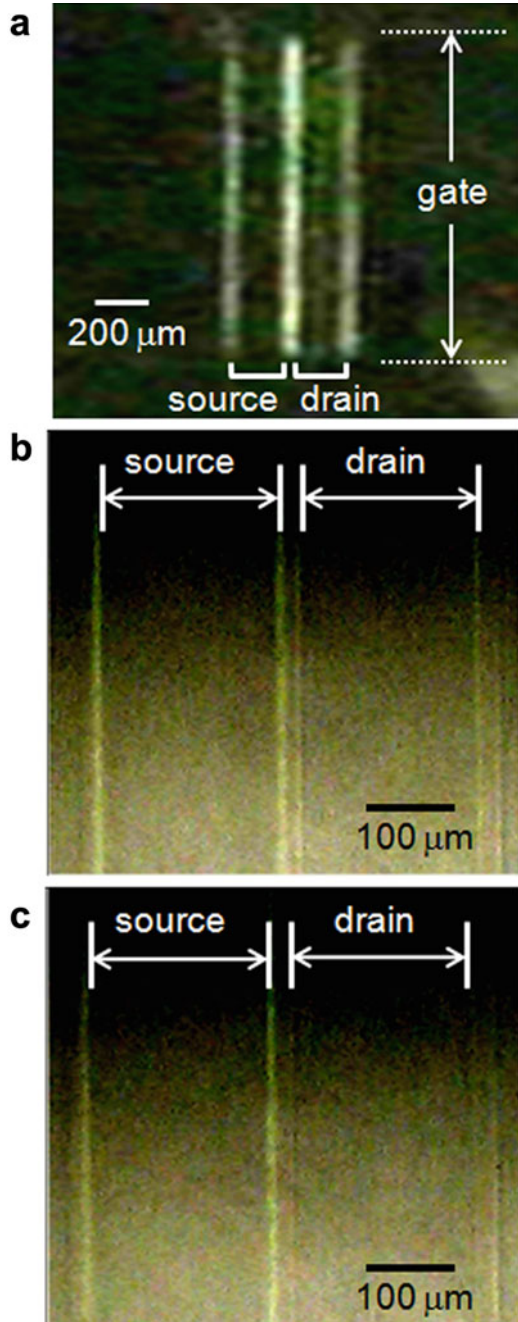


voltage-dependences in Fig. 10.6c are qualitatively explained by combining the results in Fig. 10.6a, b. However, it is noted that the light intensities at higher $|V_S|$ and $|V_D|$ in Fig. 10.6c are enhanced as compared to those estimated from the increase in Fig. 10.6a and the decrease in Fig. 10.6b.

We discuss first why the light emission is obtained at $V_S = V_D = 0$ V under AC-gate operation. As shown in Fig. 10.6a, the light intensity increases with an elevation of $|V_G|$ at $V_S = V_D = 0$ V. When the frequency f of square-wave gate biases is increased in a range of 1 Hz–20 kHz, the light intensity is also increased. Figure 10.7a shows a top-view image of the device driven at $V_S = V_D = 0$, $|V_G| = 120$ V and $f = 20$ kHz. The light emission is visible through the top-gate layer of Au crossing with a pair of the source/drain electrodes. The light emission appears not only at the center channel region but also at the left edge of the source electrode and the right edge of the drain electrode. The light intensity is higher at the center channel than at the outer edges. It suggests that the light emission occurs at the both side edges of the source and drain electrodes although the emission at the center channel is not well-resolved in this stereomicroscopic image. To clarify the appearance of light emission, the probe contact to the drain electrode was retracted so that the AC gate operates only against the source electrode. As a result, the light emission was observed only at the both side edges of the source electrode with same intensity. Similarly, the light emission occurred at the both edges of the drain electrode when the probe contact to the source electrode was retracted. These behaviors can be explained by the emission process reported for oligothiophene derivatives (Liu et al. 2010). The electron and hole carriers are alternately injected at each electrode under the AC-wave bias to the gate. In the positive half cycle of V_G , electrons are injected from the source and drain electrodes since both electrodes are grounded. When the V_G is switched to the negative half, holes are injected from both electrodes. These injected electrons (holes) recombine with the holes (electrons) accumulated in the previous half cycle of V_G . With increasing $|V_G|$ and f , the amount of accumulated carriers and the recombination cycles increase resulting in higher emission intensity. In Fig. 10.7a, the light emission is not observed in the stripe area of the source and drain electrodes of ITO. It is probably because the electric field is enhanced at the ITO step edge since the thickness of the F8T2 layer (50 nm) is considerably thin as compared to that of the ITO coating (200 nm). As a result, the carrier injection is enhanced at the step edges of ITO electrodes where a high electric field is concentrated.

In order to elucidate carrier injection and recombination dynamics, we observed time responses of light intensity with respect to the AC-gate wave. Figure 10.8a shows a time profile taken at $V_S = V_D = 0$ V with respect to the square-wave AC gate bias of $|V_G| = 120$ V and $f = 1$ kHz as is shown in Fig. 10.8e. It indicates that the light intensity rises steeply when the gate is switched to positive V_G and then gradually decays in the positive half period of V_G . On the other hand, the emission intensity appears in a sharp peak and immediately extinct when the V_G is switched to negative. It suggests that the amount of electrons accumulated in the half cycle of positive V_G is considerably smaller than that of holes accumulated in the half cycle of negative V_G . As mentioned in the Sect. 10.3.2., it is attributed to the higher

Fig. 10.7 Top-view micrographs of light emission from OLEFET with F8T2 film annealed at 350 °C under operations at $V_S = V_D = 0$ V, $|V_G| = 120$ V and $f = 20$ kHz (a), $V_S = -60$ V, $V_D = 0$ V, $|V_G| = 100$ V, $f = 20$ kHz (b) and $V_S = -60$ V, $V_D = 60$ V, $|V_G| = 100$ V, $f = 20$ kHz (c). Reproduced from Ohtsuka Y, Ishizumi A, Yanagi H (2012) Light-emitting field-effect transistors with π -conjugated liquid-crystalline polymer driven by AC-gate voltages. *Org. Electron* 13: 1710–1715 with permission from Elsevier B.V



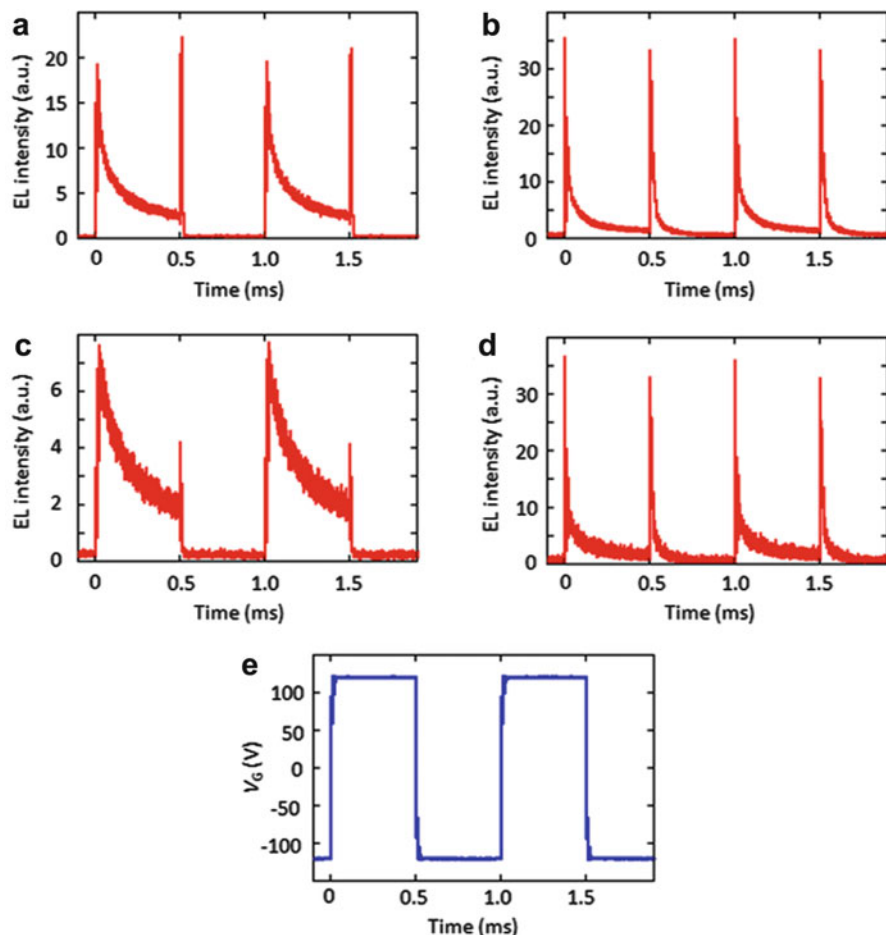


Fig. 10.8 Time responses of light intensity taken from OLEFET with F8T2 film annealed at 350 °C under operations at $V_S = V_D = 0$ V (a), $V_S = -50$ V, $V_D = 0$ V (b), $V_S = 0$ V, $V_D = 50$ V (c), $V_S = -50$ V, $V_D = 50$ V (d) with respect to square-wave form of $V_G = |120|$ V and $f = 1$ kHz (e). Reproduced from Ohtsuka Y, Ishizumi A, Yanagi H (2012) Light-emitting field-effect transistors with π -conjugated liquid-crystalline polymer driven by AC-gate voltages. *Org. Electron* 13: 1710–1715 with permission from Elsevier B.V

injection barrier for electrons than for holes owing to the HOMO/LUMO energies of F8T2 with respect to the work function of ITO source/drain electrodes. Therefore, the duration of the light intensity in the negative half cycles of V_G is very short as compared to in the positive half cycle. Figure 10.8b shows time response of light intensity when the V_S is biased to -50 V. The duration of light emission in the positive half cycles of V_G is shortened while that in the negative half cycles is elongated. The negative bias of V_S increases the electron injection from the source electrode in the positive V_G period while decreases the hole injection from the

source electrode in the negative V_G period. On the other hand, the durations of light emission in the positive and negative V_G cycles are elongated and shortened, respectively, when the V_D is biased to 50 V, as shown in Fig. 10.8c. The positive bias of V_D remarkably decreases the peak intensities when the V_G polarity is switched since the amount of electrons injected from the drain electrode is decreased. Figure 10.8d shows the time response of light intensity when the V_S and V_D are biased to -50 and 50 V, respectively. The peak intensity and duration of light emission are similar to that taken at $V_S = -50$ and $V_D = 0$ V (Fig. 10.8b) suggesting that the electron injection from the negatively biased source electrode is crucial for the light-emitting recombination.

Such dependences of EL characteristics on magnitude and polarity of V_S and V_D under AC-gate operations are further discussed by observing high magnification images of light emission. Figure 10.7b shows an optical micrograph of the device taken at $V_S = -60$ V, $V_D = 0$ V, $|V_G| = 100$ V, $f = 20$ kHz. It shows that the light emission is observed at both side edges of the source and drain electrodes. The light intensity at both edges of the source electrode is higher than that of the drain electrode edges since the negative V_S enhances the electron injection from the source electrode edges. Figure 10.7c shows an image taken at $V_S = -60$ V, $V_D = 60$ V, $|V_G| = 100$ V, $f = 20$ kHz. The light emission is not observed at both edges of the drain electrode while the light intensity at the right-side edge of the source electrode is slightly higher than that at the left-side edge emission. This enhanced emission is ascribed to recombination between electrons injected at the right-side edge of the source and holes which are injected from the drain electrode and transported along the channel. At $V_D = 60$ V, there are few electrons at the drain electrode edge, therefore, the holes are driven to move toward the source electrode biased at $V_S = -60$ V. These findings suggest that the present AC-gate polymer OLEFET can be effectively operated by making the best use of this channel recombination. If interdigitated source/drain electrodes are constructed, enhanced light emission will be obtained at both edges of all source electrodes.

As is expected from above-mentioned time responses and microscopic observations, the light-emitting behavior under AC-gate operations is modified when a sinusoidal AC wave is used as the gate bias. The light intensity in both positive and negative half cycles was decreased than in the case of the square-wave application. The gradual switching of the V_G decreases light-emitting recombination since the accumulation and injection of opposite carries are reduced when the V_G is continuously switched. Time-dependent EL intensity and current flow have been reported for the TPCO-crystal OLEFET operated with sinusoidal AC-gate voltages (Yamao et al. 2008). The time response of the present device operated with a sinusoidal wave ($V_G = |120|$ V and $f = 10$ kHz) at $V_S = V_D = 0$ V resembled this literature results at high f . The light intensity increases in the positive half cycles of V_G while the currents flow only in the negative half cycles of V_G . It suggests that the current is dominated by the holes transported in the channel while the light emission is governed by the injected electrons.

Finally, we compared light-emitting performances of the OLEFETs with F8T2 films annealed at different temperatures in order to examine the effect of crystalline

states as described in Sects. 10.2.3. and 10.3.2. The AC-gate operation was carried out with a square-wave bias of $|V_G| = 100$ V and $f = 20$ kHz for the F8T2 films annealed at 250, 290, and 350 °C. The V_D was set at 0 V while the V_S was at -60 V to enhance the electron transport. The EL intensity increased in the order of annealing temperature of $290 < 250 < 350$ °C. This order coincides with the order of μ_e as shown in Fig. 10.5a. It suggests again that the electron carrier generation is crucial for ambipolar OLEFET performances. Time responses of the EL intensity were also compared for the F8T2 films annealed at 250, 290, and 350 °C. The AC-gate operation was carried out at $-V_S = V_D = 50$ V with a square-wave gate of $|V_G| = 100$ V and $f = 1$ kHz. The time profiles of all films indicate that the light intensity rises steeply when the V_G is switched to positive and then quickly decays in the half period of positive V_G . It indicates again that the electrons injected from the source electrode recombine with the holes accumulated in the previous half cycle of negative V_G for all three devices. When the V_G is switched to negative, the sharp EL peak similarly appears but it immediately quenched in the negative period of V_G since the accumulated electrons in the previous cycle of positive V_G is less persistent. The EL intensity peak in the positive V_G is much higher than that in the negative V_G for the films annealed at 250 and 350 °C. However, this relative difference between the EL peak intensities in the positive and negative V_G cycles is less remarkable for the film annealed at 290 °C although its absolute EL intensity is much lower. It is probably because the electrons trapped at the grain boundaries in the channel contribute to the recombination with holes injected when the V_G is switched to negative. Consequently, the homogeneous F8T2 film obtained by annealing at isotropic temperature of 350 °C is most suitable for light-emitting layer of the present liquid-crystalline OLEFET under AC-gate operation.

10.4 Conclusions

Bottom-contact/top-gate OLEFETs were fabricated with a light-emitting π -conjugated liquid-crystalline thiophene/fluorene co-polymer, F8T2. Thin film structure and transistor characteristics of F8T2 were comparably characterized for spin-coating films which were annealed at different temperatures and quenched to room temperature. The amorphous films annealed far below the thermotropic transition temperature exhibited fully hole-transporting unipolar characteristics owing to random conformation of the F8T2 chains. By annealing at 250 °C close to the transition temperature, the film started to have ambipolar characteristics due to electron transport among partially aligned molecular chains. With increasing annealing temperature at 290 °C, the microcrystalline structure quenched from the nematic phase remarkably reduced the ambipolar transport probably due to electron trapping at the grain boundaries. On the other hand, when the F8T2 film was quenched from the isotropic melt at 350 °C, the device with less-crystallized homogeneous structure showed the highest ambipolar performance.

The fabricated OLEFETs exhibited light emission under AC-gate operations at different conditions of V_S , V_D , $|V_G|$ and f . Light emission was observed at both edges of the source and drain electrodes even at $V_S = V_D = 0$ V by applying square-wave voltages to the gate. According to the polarity switch of AC-gate voltages, electrons and holes are alternately injected from both source and drain electrodes, and recombine with the opposite carriers injected in the previous half cycle of V_G . The light emission is dominated by electron injection due to a higher barrier for electrons from the ITO electrode to the F8T2 film even if the electron and hole mobilities are in the same order of magnitude. As a result, the light intensity increased by applying negative V_S while V_D was kept at 0 V. On the other hand, the light emission is suppressed by applying positive V_D at $V_S = 0$ V. When the V_S and V_D were simultaneously biased negative and positive, respectively, the light intensity was enhanced in the center channel region by recombination between the holes transported from the drain and the electrons injected at the source electrode edge. Further progress of ambipolar liquid-crystalline polymer OLEFETs will be developed with well-designed electronic energy of materials and controlled crystalline morphology. The AC-gate operation with optimized device structures may lead to a new class of flexible light-emitting devices.

This chapter was written by reproducing and rearranging the texts and figures published in Refs. by Ohtsuka et al. (2012) and Muneishi et al. (2014).

This work was supported by Grant-in-Aid for Scientific Research (C) No.22550163 from the Japan Society for the Promotion of Science (JSPS). This work was also supported by the Green Photonics Project of Nara Institute of Science and Technology. The authors thank Mr. Fujiwara, Nara Institute of Science and Technology for his experimental support.

References

- Ahles M, Hepp A, Schmechel R, Segern H (2004) Light emission from a polymer transistors. *Appl Phys Lett* 84:428–430
- Baldo MA, Holmes RJ, Forrest SR (2002) Prospects for electrically pumped organic lasers. *Phys Rev B* 66:035321
- Broughes JH, Bradley DD, Brown AR, Marks RN, Mackay K, Friend RH, Burn PL, Holmes AB (1990) Light-emitting diodes based on conjugated polymers. *Nature* 347:539–541
- Fichou D, Delysse S, Nunzi JM (1997) First evidence of stimulated emission from a monolithic organic single crystal: α -octithiophene. *Adv Mater* 9:1178–1181
- Hamasaki T, Morimune T, Kajji H, Minakata S, Tsuruoka R, Nagamachi T, Ohmori Y (2009) Fabrication and characteristics of polyfluorene based organic photodetectors using fullerene derivatives. *Thin Solid Films* 518:548–550
- Hepp A, Heil H, Weise W, Ahles M, Schmechel R, von Seggern H (2003) Light-emitting field-effect transistor based on a tetracene thin film. *Phys Rev Lett* 91:91157406
- Hide F, Díaz-García MA, Schwartz BJ, Andersson MR, Pei Q, Heeger AJ (1996) Semiconducting polymers: a new class of solid-state laser materials. *Science* 273:1833–1836
- Horowitz Q, Valat P, Garnier F, Kouki F, Wintgens V (1998) Photoinduced spontaneous and stimulated emission in sexithiophene single crystals. *Opt Meter* 9:46–52

- Ichikawa M, Hibino R, Inoue M, Haritani T, Hotta S, Araki K, Koyama T, Taniguchi Y (2005) Laser oscillation in monolithic molecular single crystals. *Adv Mater* 17:2073–2077
- Kajii H, Koiwai K, Hirose Y, Ohmori Y (2010) Top-gate-type ambipolar organic field-effect transistors with indium-tin-oxide drain/source electrodes using polyfluorene derivatives. *Org Electr* 11:509–513
- Kelly TW, Boardman LD, Dunbar TD, Muyres DV, Pellerite MJ, Smith TP (2003) High-performance OFETs using surface-modified alumina dielectrics. *J Phys Chem B* 107:5877–5881
- Kinder L, Kanicki J, Swensen J, Petroff P (2004) *Synth Met* 146:181–185
- Koiwai K, Kajii H, Ohmori Y (2011) Effects of film morphology on ambipolar transport in top-gate-type organic field-effect transistors using poly(9,9-dioctylfluorene-co-bithiophene). *Synth Met* 161:2107–2112
- Kudo K, Yamashina M, Moriizumi T (1984) Field effect measurement organic Dye films. *Jpn J Appl Phys* 23:130
- Liu X, Wallmann I, Boudinov H, Hansen JK, Schiek M, Lutzen A, Rubahn HG (2010) AC-biased organic light-emitting field-effect transistors from naphthyl end-capped oligothiophenes. *Org Electr* 11:1096–1102
- Muneishi T, Ishizumi A, Yanagi H (2014) Annealing effect on light-emitting FET characteristics of π -conjugated liquid crystalline polymer. *Jpn J Appl Phys* 53:01AB17
- Ohtsuka Y, Ishizumi A, Yanagi H (2012) Light-emitting field-effect transistors with π -conjugated liquid-crystalline polymer driven by AC-gate voltages. *Org Electr* 13:1710–1715
- Sakanoue T, Fujiwara E, Yamada R, Tada H (2004) Visible light emission from polymer-based field-effect transistors. *Appl Phys Lett* 84:3037–3039
- Sawabe K, Imakawa M, Nakano M, Yamao T, Hotta S, Iwasa Y, Takenobu T (2012) Current-confinement structure and extremely high current density in organic light-emitting transistors. *Adv Mater* 24:6141–6146
- Sheats JR, Antoniadis H, Hueschen M, Leonard W, Miller J, Moon R, Roitman D, Stocking A (1996) Organic electroluminescent devices. *Science* 273:884–888
- Swensen J, Soci C, Heeger AJ (2005) Light emission from an ambipolar semiconducting polymer field-effect transistor. *Appl Phys Lett* 87:253511
- Takenobu T, Bisri SZ, Takahashi T, Yahiro M, Adachi C, Iwasa Y (2008) High current density in light-emitting transistors of organic single crystals. *Phys Rev Lett* 100:066601
- Takeya J, Yamagishi M, Tominari Y, Hirahara R, Nakazawa Y, Nishikawa T, Kawase T, Shimoda T, Ogawa S (2007) Very high-mobility organic single-crystal transistors with in-crystal conduction channels. *Appl Phys Lett* 80:102120
- Tang CW (1986) Two-layer organic photovoltaic cells. *Appl Phys Lett* 48:183–185
- Tang CW, VanSlyke SA (1987) Organic electroluminescent diodes. *Appl Phys Lett* 51:913–915
- Tessler N, Denton GJ, Friend RH (1996) Lasing from conjugated-polymer microcavities. *Nature* 382:695–697
- Tsumura A, Koezuka H, Ando T (1986) Macromolecular electronic device: field-effect transistor with a polythiophene thin film. *Appl Phys Lett* 49:1210–1212
- Yamane K, Yanagi H, Sawamoto A, Hotta S (2007) Ambipolar organic light emitting organic field effect transistor with modified asymmetric electrodes. *Appl Phys Lett* 90:162108
- Yamao T, Shimizu Y, Terasaki K, Hotta S (2008) Organic light-emitting field-effect transistors operated by alternating current gate voltages. *Adv Mater* 20:4109–4112
- Yamao T, Terasaki K, Shimizu Y, Hotta S (2010) Organic-crystal light-emitting field-effect transistors driven by square-wave gate voltages. *J Nanosci Nanotechnol* 10:1017–1020
- Zaumseil R, Friend RH, Sirringhaus H (2006) Spatial control of the recombination zone in an ambipolar light-emitting organic transistor. *Nat Mater* 5:69–74
- Zheng Z, Yim KH, Saifullah MSM, Welland ME, Friend RH, Kim JS, Huck WTS (2007) Uniaxial alignment of liquid-crystalline conjugated polymers by nanoconfinement. *Nano Lett* 7:987–992